A Hematite Photoelectrode Grown on Porous and Conductive SnO_2 Ceramics for Solar-Driven Water Splitting

Alexander N. Bondarchuk [a]*, Iván Corrales-Mendoza [a], Sergio A. Tomás [b], Frank Marken [c]

[a] Technological University of Mixteca, Huajuapan 69000, Oaxaca, Mexico
[b] Department of Physics, CINVESTAV, Av Instituto Politécnico Nacional 2508, San Pedro Zacatenco, Gustavo A. Madero, Ciudad de México, C.P. 07360
[c] Department of Chemistry, University of Bath, Bath BA2 7AY, UK

Abstract

Photoelectrochemical water splitting using solar energy is a highly promising technology to produce hydrogen, which offers an environmentally friendly and renewable fuel with high-energy capacity. This approach requires the development of appropriate photo-electrode materials, which are low cost and applicable for the fabrication of large area electrodes. In this work, hematite photoelectrodes are grown onto highly-conductive and porous SnO_2 (Sb-doped) ceramic substrates by aerosol assisted chemical vapour deposition (AA-CVD). For such photoelectrodes, the photocurrent value of 2.8 mA cm^{-2} in aqueous 0.1 M NaOH under blue LED illumination (λ= 455 nm; 198 mW cm^{-2}) at 1.23 V vs. RHE (reversible hydrogen electrode) is achieved. This relatively good photoelectrochemical performance of the photoelectrode is achieved despite the simple fabrication process. Good performance is suggested to be related to the three-dimensional morphology of the ceramic substrate resulting in excellent light-driven charge carrier harvesting. The porosity of the ceramic substrate allows growth of the photoactive layer (SnO_2-grains covered by hematite) to a depth of some micrometers, whereas the thickness of Fe_2O_3-coating on individual grains is only about 100-150 nm. This architecture of the photoactive layer assures a good light absorption and creates favourable conditions for charge separation and transport.

Keywords: Hematite, Ceramics, Photoanode, Water splitting, Solar energy

1. Introduction

The conversion and storage of solar energy in the form of hydrogen (or other) fuel, carried out by photoelectrochemical (PEC) water splitting [1] is a highly promising technology to produce environmentally friendly and renewable fuels with high-energy capacity and low carbon emission [2-5]. The technology is based on photo-electrolysis of water into O_2 (at the photo-anode) and H_2 (at the photo-cathode) on the surface of suitable photo-active materials under solar illumination. This approach requires the development of appropriate photo-electrode materials, which should satisfy a number of conditions such as (i) low cost of production, (ii) suitability for fabrication of large area electrodes, (iii) strong absorption in the right region of the spectrum of solar radiation, (iv) a suitable band edge position for reduction/oxidation of water, and (v) high chemical stability for long term operation in aqueous environments [1-8]. To find a photo-electrode material suitable for commercial production of hydrogen, many

chemical compounds and materials have been engineered and tested [7-43]. However, this task has not been totally resolved at the present time.

A promising candidate for photo-anode applications is α-Fe_2O_3 (hematite), which has a suitable band gap (~2 eV) capable of absorbing up to 40% (or higher in tandem cells) of the incident solar light [13]. Hematite possesses good stability in harsh aqueous media, is non-toxic, low cost, and is earth abundant. The theoretical maximum solar-to-hydrogen efficiency for hematite can reach 15%, while 10% is already enough for practical applications [4]. In theory, this material can produce a photocurrent density of ca. 4 mA cm^{-2} (for single pass flat interfaces) or up to ca. 12 mA cm^{-2} (for nano-structured interfaces) under AM 1.5 solar spectral illumination [6]. However, poor electrical conductivity of un-doped hematite (ca. 10^{-14} $ohm^{-1}cm^{-1}$ [4]), fast recombination of photo-generated electrons and holes [12,14], a short hole diffusion length (~2-4 nm [15] or even 0.5-1.5nm [16]) and slow surface kinetics associated with the formation of oxygen [17] result in these photocurrent values not being achieved in practice.

To surmount these drawbacks of hematite, a number of approaches have been attempted, including doping of hematite to increase conductivity [2], application of nano-textured conductive substrates for more efficient charge collection [18], the integration of an ultrathin under-layer at the interface of substrate and hematite film [16,19], heterojunctions to enhance a charge carrier collection [20,21], surface/interface passivation layers for reduced surface/interface charge recombination [22], and catalyst adsorption for accelerated interfacial water oxidation kinetics [23-25]. The highest photocurrent density (4.68 mA cm^2 in aqueous 1 M NaOH at 1.23V vs. RHE under AM 1.5 illumination) has been reported for hematite nanostructured photoanode synthesized via the electrochemical method and modified with Ag nanoparticles and Co–Pi cocatalyst [26]. Grätzel and coworkers reported 2.2 mA cm^{-2} under similar conditions [27] and more recently 3.12 mA cm^{-2} for surface treated hematite [28]. However, for the photo-anode of pristine hematite, usually the photocurrent density does not exceed 1 mA cm^{-2} [2-5, 29-31].

To fully exploit the potential of hematite in PEC water splitting, harvesting of solar light by the photoanode should be the fullest possible, whilst fabrication methods should be based on low cost procedures and materials. We set out to investigate whether this condition can be met when a thin Fe_2O_3-film is deposited over porous and conductive substrate formed from SnO_2 ceramics. This approach to obtain an improved hematite photoelectrode can be considered as a variant of the “host-guest” strategy [32-35], which is based upon a 3D porous support material for majority carrier conduction (“host”) and has many thin layers of the photoactive material (“guest”).

The choice of SnO_2 as the main component of ceramics for substrate has been made considering the reports in literature that Sn-doping of hematite results in photocurrent increases [36-40]. Sn dopant serves as an electron donor and increases the charge-carrier density of hematite [38]. Therefore, heat treatment of Fe_2O_3 film deposited on SnO_2 ceramics can lead to Sn^{4+} substitution at Fe^{3+} sites in hematite and give a positive

effect on photocurrent. SnO_2 is an n-type semiconductor, and so its grains form a conductive path for electrons through the ceramic substrate.

To test this new and relatively simple approach to photoelectrode production (photocatalytic film deposition onto volume- and porous conductive ceramics), porous SnO_2-Sb_2O_5 ceramics were synthesized as the substrate and the hematite coating was applied by Aerosol Assisted Chemical Vapour Deposition (AA-CVD). The novelty of our work is based on using simple, conductive, and porous volume ceramics as substrate to host the hematite coating. To the best of our knowledge, such photoanodes are reported here for the first time. The three-dimensional morphology and the porosity of ceramics result in a strongly enhanced harvesting of solar light without additional complexity in the fabrication process. Moreover, visible solar radiation can penetrate/diffuse into volume of such ceramic substrate or at least into its near-surface layer, because the band-gap of SnO_2 is about 3.6 eV [31], which makes this oxide transparent for visible solar light (360-740 nm). In this report, the results for electrochemical testing, as well as structural and morphological characterization of the new photoelectrodes are presented and discussed. Further optimization of the ceramic substrate and the hematite coating for further improvements in the photoelectrode will be possible in the future.

2.Material and methods

Ceramic substrates in the form of discs (radius 9 mm and height 3-4 mm) were prepared from 99 mol% SnO_2 – 1 mol% Sb_2O_5 ceramics by the conventional oxide mixture method using distilled water [44]. The powders of tin and antimony oxides (99 and 1 mol% respectively) were mixed and milled in an agate mortar for 45 min with distilled water. The donor dopant of Sb_2O_5 was used to improve conductivity of the SnO_2-ceramic substrate. The purity of starting oxides was not less than 99.5%. After wet-milling and drying (120°C for 2h), the resulting powder was pressed into discs 9 mm in diameter and 3-5 mm in thickness at an axial pressure of approximately 150 MPa using hydraulic CARVER press. Next, the pressed oxides were sintered in air at 1300°C for 1 h with a slow heating and cooling rate of 2 degree/min.

Iron(III) 2,4-petaneodinate from Sigma-Aldrich dissolved in ethyl alcohol (1.13 mol/L) was used as a hematite precursor. The film deposition was performed in a cold wall reactor at 350°C and atmospheric pressure using N_2 as carrier gas at a flow rate of 1.38 L/min to deliver the hematite precursor aerosol produced by ultrasonic nebulization to the substrate. The samples were subsequently annealed at 550°C for 1 h in air with a heating/cooling rate of 3°C/min in a Thermolyne furnace. After that, the Ag electrode was printed with quick-drying silver paste (05002-AB, SPI Supplies) on the side of the ceramic substrate not covered by hematite film and dried at 50°C for 2h. Then this Ag electrode was soldered to an insulated wire, and the contact area was covered with silicone glue (Fig.1, see the inset). The geometric surface areas of hematite photoanode grown on the ceramic substrate and on the ITO substrate were 0.62 cm^2 and 1.5cm^2, respectively. These values were used to calculate the photocurrent density of different electrodes.

Electrochemical measurements were performed with a Keithley 2410 unit connected as a potentiostat in the three-electrode configuration (a Pt-wire counter electrode, the hematite photoanode as the working electrode with area of 0.62 cm^2, and a Radiometer REF201 reference electrode with a saturated KCl reference system). Potentials versus reversible hydrogen electrode (RHE) were calculated using the Nernst equation $E_{RHE} = E_{Ag/AgCl} + 0.0591 \times pH + 0.1976\,V$. Electrolyte solutions were 0.1 M NaOH in demineralised water ($pH = 12.65$). The light chopping frequency was set at 0.03 Hz. Light was generated by the blue LED (455 nm, Thorlabs M455L2) emitting radiation with the power density of 198 mW cm^{-2} at the wavelength of 455 nm. The power density of LED radiation was estimated by the laser power meter OPHIR with a PD200W-SH head having the aperture of 1 cm^2.

The incident photon-to-current efficiency (IPCE) was calculated using the equation $IPCE(\lambda) = \left|J_{ph}(mA/cm^2)\right| \times 1239.8(V \times nm) \Big/ \left[P_{light}(mW/cm^2) \times \lambda(nm)\right]$, where J_{ph} - was the photocurrent density registered for the photoelectrode under light with the wavelength λ and the intensity P_{light}.

The current-voltage characteristic for SnO_2-Sb_2O_5 ceramics was recorded in air by two-probe method utilizing a Keithley-2410 source meter. For this experiment, the Ag electrodes were formed on both sides of the ceramic substrate. The dc conductivity (g) of ceramics was estimated from the expression $g = Gd/S$ where G is the dc conductance of sample, and d and S are the thickness and the cross-section of a sample, respectively.

The morphology of the materials was evaluated by scanning electron microscopy (SEM, TESCAN Vega 3) with the Bruker detector for energy-dispersive X-ray spectroscopy (EDS). The X-ray diffraction (XRD) pattern was recorded using a Bruker AXS D8 Advance diffractometer with CuKα radiation (λ=1.542 Å) operated at 40 kV and 30 mA. Phase identification was performed using the ICDD PDF-2 database (ICDD – International Centre for Diffraction Data, Newtown Square, PA). The photoacoustic absorption spectra of the synthesized materials were obtained in the spectral region 400-850 nm by the use of a conventional photoacoustic spectrometer equipped with a high power 1000 W Xenon lamp (Oriel, 6271) [45]. The radiation from the lamp was focused onto a monochromator (Oriel, 77250) and the monochromatic beam then passed through a variable-frequency light chopper kept at 17 Hz. With the help of optical fibers, the monochromatic light was focused onto the samples placed into a closed photoacoustic cell fitted with an electret microphone. The photoacoustic signal was sent to a lock-in amplifier (Stanford Research Systems, SR850).

The density (D) of SnO_2-Sb_2O_5 ceramics used for substrates was estimated by Archimedes' principle: $D = D_0 m_1/(m_1 - m_2)$ where D_0 is the density of water; and m_1 and m_2 are the mass of sample in air and in water, respectively.

3. Results and Discussion

After annealing at 550°C for 1 h in air, the hematite films on ceramic substrates have a bright orange colour typical for α-Fe_2O_3 (Fig. 1, see the inset). The bare ceramic substrate has a dark grey colour. The XRD pattern (Fig. 1) shows the presence of the rhombohedral hematite phase in and tetragonal SnO_2. The Sb-phases are not detected because their concentration is below the detection limit by XRD.

Scanning electron microscopy (SEM) images for the front side of photoelectrode (ceramic substrate covered by hematite) and for the reverse side (bare ceramic) are shown in Fig. 2a and Fig.2b, respectively. As seen in Fig.2b, the ceramic substrate possesses high porosity. The density of tin dioxide ceramics used for the substrate is about 5.77 g cm^{-2}, while the theoretical density of SnO_2 is 6.95 g cm^{-3}. A high porosity of material is favourable for penetration of the hematite precursor and growth of Fe_2O_3 films on grains within the bulk of the ceramic substrate. This was confirmed by the energy-dispersive X-ray spectroscopy (EDS) data presented in Fig.2.

The EDS elemental map of the Fe distribution in cross-section of photoanode shows a layer with high concentration of Fe which formed on the surface of ceramic substrate and in its volume, near substrate surface (Fig.2d). The thickness of this photoactive layer (a bright red area in Fig.2d) varies and is in the range of 3-20 μm. As can be seen in Fig.2d, there are Fe-atoms throughout the entire volume of the ceramic substrate. However, their number is much higher in the area near the surface of the photoelectrode (Fig.2d). We conclude that a photoactive layer is formed mainly on surface of the ceramic substrate and in its subsurface volume to a depth of about 3-20 μm. The size of the SnO_2 grains covered by hematite is about 500 nm (Fig. 2a), whereas the grains without Fe_2O_3-coating in ceramics on the reverse side of photoelectrode are smaller and about 200-300 nm (Fig. 2b). This suggests that the thickness of hematite film on the grains is about 100-150 nm.

Cyclic voltammograms recorded for the hematite photoanode immersed in 0.1 M NaOH electrolyte under chopped blue light of LED Thorlabs M455L2 (198 mW cm^{-2} at λ=455nm) exhibited a photocurrent value of 2.8 mA cm^{-2} at 1.23V versus RHE (Fig.3, curve 1). These photocurrent values are reproduced as well if light of the LED is permanently turned on (Fig.3, curve 3). The reported photocurrent value of 2.8 mA cm^{-2} at 1.23 V vs. RHE corresponds to the IPCE value of 3.8% estimated at the wavelength of 455 nm.

To be sure that PEC performance of the photoelectrode is not a result of some photoelectric processes in the SnO_2-Sb_2O_5 ceramic, cyclic voltammorgrams for ceramic substrate not covered by hematite were recorded (Fig.4). In this case, only a relatively low photocurrent about 7.5μA cm^{-2} at 1.23 V versus RHE is observed (Fig.4, see inset). Thus, the PEC performance of the obtained photoelectrode is related to its hematite coating. As seen in Fig.4, dark current in SnO_2-Sb_2O_5 ceramics without hematite is relatively high and is about 0.1 mA cm^{-2} at 1.23 V vs. RHE. This shows that SnO_2-Sb_2O_5 ceramic is a good conductor. The current-voltage characteristic registered for SnO_2-Sb_2O_5 ceramics in air by two-probe method is linear and the conductivity value is about 1.7 $Ohm^{-1}cm^{-1}$.

To find out the contribution of the ceramics morphology to the PEC performance of the hematite photoanode, a hematite film is grown on glass substrates coated with tin-doped indium oxide (ITO) by AA-CVD under the same conditions. For the hematite photoelectrode grown on ITO, the photocurrent density is only about 0.07 mA cm^{-2} at 1.23 V vs. RHE (Fig.5, curve 1) and the corresponding IPCE value at the wavelength of 455 nm is about 0.1%. These data show that higher PEC performance of the hematite photoanode grown on ceramics is achieved due to specific properties of the substrate.

The SEM and EDS data suggest that the high photocurrent exhibited by the hematite photoelectrode grown on SnO_2-Sb_2O_5 ceramics can be attributed to its excellent light harvesting caused by 3D morphology of substrate. The porous photoactive layer of several micrometres thick (the bright red area in Fig.2d) can harvest solar light very well, while its thickness (3-20 µm) does not affect diffusion and recombination of photo-generated charge carriers in hematite, because the Fe_2O_3-coating on individual ceramic grain remains thin (about 150 nm or less). In additional, good harvesting of light with this photoelectrode is caused as well by small grain sizes (200-500 nm) in SnO_2 ceramics, which are comparable to wavelength of visible solar radiation (360-740 nm). Such a morphology of the photoactive layer results in a good harvesting of visible solar light, and so a high photocurrent density is observed.

Optical absorption properties of the Fe_2O_3 electrodes grown on the ceramic substrate and on the ITO are estimated from the data of photoacoustic spectroscopy (Fig.6). The hematite photoanode grown on the ceramic substrate, exhibits improved harvesting of photons (of about 2 eV) when compared to the electrode grown on the ITO substrate (Fig. 6, curve 2 and 3). The estimation of the band gap based on these spectra suggests a value of approximately 1.9 eV for hematite on the ITO substrate (Fig. 6, curve 3). This value is in good agreement with literature values of 1.9–2.5 eV [46–48].

4. Conclusions

Hematite photoelectrodes grown on highly-conductive and porous SnO_2 (Sb-doped) ceramic substrates by AA-CVD technique are reported. Relatively high PEC performance of these photoanodes (2.8 mA cm^{-2} at 1.23 V vs. RHE) is attributed to excellent light harvesting of the photoactive layer (SnO_2-grains covered by hematite), which is porous and grows in substrate volume to a depth of about 3-20 µm, whereas the thickness of Fe_2O_3-coating on individual grains is only about 100-150 nm. This architecture of the photoactive layer assures a good light absorption and creates favourable conditions for charge separation and transport. This combination of photoelectric properties is achieved due to using porous and conductive SnO-Sb_2O_5 ceramics as substrate.

The results reported here show that an application of conductive and porous ceramics as substrate for photocatalytic materials can be promising to achieve enhanced photocurrents for hematite photoelectrodes. In contrast, with nano-textured substrates, the preparation of these ceramic substrates is easier and cheaper, and this can be important for the fabrication of large area photoelectrodes for practical applications. Further engineering of ceramic substrate (for example doping, heat

treatment, method of synthesis) will lead to further improvements in the PEC performance of photocatalytic coating.

Acknowledgements

The authors thank Prof. L. Peter for discussion and support. This study was supported by the National Science and Technology Council of Mexico (CONACYT, #280373 and #259705) and funding from the PRODEP by project number UTMIX-PTC-054 to assemble AA-CVD system. This support is gratefully acknowledged. The authors are grateful to Dr. Erick Adrián Juárez Arellano for his help with X-ray analysis.

References

[1] Peter LM. Photoelectrochemical water splitting. A status assessment. Electroanalysis 2015; 27:864-7.
[2] McKone JR, Lewis NS, Gray HB. Will Solar-Driven Water-Splitting Devices See the Light of Day? Chem. Mater. 2014; 26:407−7.
[3] Orlandi M, Mazzi A, Arban G, Bazzanella N, Rudatis P, Caramori HB, et al. On the effect of Sn-doping in hematite anodes for oxygen evolution. Electrochimica Acta 2016; 214:345-8.
[4] Tamirat G, Rick J, Dubale AA, Sub W-N, Hwang B-J. Using hematite for photoelectrochemical water splitting: a review of current progresses and challenges. Nanoscale Horiz. 2016; 1:243-14.
[5] Joy J, Mathew J, George SC. Nanomaterials for Photoelectrochemical Water Splitting- Review. Int J. Hydrogen Energy 2018; 43:4804-4.
[6] Wang K.X, Yu Z, Liu V, Brongersma ML, Jaramillo TF, Fan S. Nearly total solar absorption in ultrathin nanostructured iron oxide for efficient photoelectrochemical water splitting. ACS Photonics 2014; 1:235-5.
[7] He Y, Hamann T, Wang D. Thin film photoelectrodes for solar water splitting. Chem. Soc. Rev. 2019; 48:2182-12.
[8] Fang S, Hu YH. Recent progress in photocatalysts for overall water splitting. Int J Energy Res. 2018; 43:1082–17.
[9] Qureshy AMMI, Ahmed M, Dincer I. Performance assessment study of photo-electro-chemical water-splitting reactor designs for hydrogen production. Int J. Hydrogen Energy 2019; 44:9237-10.
[10] Pawar GS, Elikkottil A, Pesala B, Tahir AA, Mallick TK. Plasmonic nickel nanoparticles decorated on to $LaFeO_3$ photocathode for enhanced solar hydrogen generation. Int J. Hydrogen Energy 2019; 44:578-6.
[11] Lin YXQ, Ahmed R, Hoglund ER, Zangari G. Synthesis of TiO_2-based nanocomposites by anodizing and hydrogen annealing for efficient photoelectrochemical water oxidation. J. Power Sources 2019; 410:59-9.
[12] van de Krol R, Liang Y, Schoonman J. Solar hydrogen production with nanostructured metal oxides. J. Mater. Chem. 2008; 18:2311-5.
[13] Peter LM. Energetics and kinetics of light-driven oxygen evolution at semiconductor electrodes: the example of hematite. J. Solid State Electrochem. 2013; 17:315-11.

[14] Wijayantha KGU, Saremi-Yarahmadi S, Peter LM. Kinetics of oxygen evolution at α-Fe_2O_3 photoanodes: a study by photoelectrochemical impedance spectroscopy. Phys. Chem. Chem. Phys. 2011; 13:5264–6.
[15] Kennedy JH, Frese KW. Photooxidation of Water at α - Fe_2O_3 Electrodes. J. Electrochem. Soc. 1978; 125:709-5.
[16] Le Formal F, Sivula K, Grätzel M. The Transient Photocurrent and Photovoltage Behavior of a Hematite Photoanode under Working Conditions and the Influence of Surface Treatments. J. Phys. Chem. C 2012; 116:26707-13.
[17] Cummings CY, Marken F, Peter LM, Wijayantha KGU, Tahir AA. New insights into water splitting at mesoporous α-Fe_2O_3 films: A study by modulated transmittance and impedance spectroscopies. J. Am.Chem. Soc. 2012; 134:1228–6.
[18] Wheeler DA, Wang G, Ling Y, Li Y, Zhang JZ. Nanostructured hematite: synthesis, characterization, charge carrier dynamics, and photoelectrochemical properties. Energy & Environmental Science 2012; 5:6682-4.
[19] Wanga D, Zhang X-T, Sun P-P, Lu S, Wanga L-L, Wei Y-A, et al. Enhanced photoelectrochemical water splitting on hematite thin film with layer-by-layer deposited ultrathin TiO_2 underlayer, Int J. Hydrogen Energy 2014; 3:16212-7.
[20] Boudoire F, Toth R, Heier J, Braun A, Constable EC. Photonic light trapping in self-organized all-oxide microspheroids impacts photoelectrochemical water splitting. Energy Environ. Sci. 2014; 7: 2680-8.
[21] Cai J, Li S, Pan H, Liu Y, Qin G, c-In_2O_3/α-Fe_2O_3 heterojunction photoanodes for water oxidation. J. Mater. Sci. 2016; 51:8148–7.
[22] Tamirat AG, Su WN, Dubale AA, Pan CJ, Chen HM, Ayele DW, et al. Efficient photoelectrochemical water splitting using three dimensional urchin-like hematite nanostructure modified with reduced graphene oxide. J. Power Sourc. 2015; 287:119-9.
[23] Moir JW, Sackville EV, Hintermair U, Ozin GA. Kinetics versus Charge Separation: Improving the Activity of Stoichiometric and Non-Stoichiometric Hematite Photoanodes Using a Molecular Iridium Water Oxidation Catalyst. J. Phys. Chem. C. 2016; 120:12999-13.
[24] Zhong DK, Cornuz M, Sivula K, Grätzel M, Gamelin DR. Photo-assisted electrodeposition of cobalt–phosphate (Co–Pi) catalyst on hematite photoanodes for solar water oxidation. Energy Environ. Sci. 2011; 4:1759-5.
[25] Riha SC, Klahr BM, Tyo EC, Seifert S, Vajda S, Pellin MJ, et al. Atomic Layer Deposition of a Submonolayer Catalyst for the Enhanced Photoelectrochemical Performance of Water Oxidation with Hematite. ACS Nano 2013; 7:2396-9.
[26] Perakiatkhajohn P, Yun J-H, Chen H, Lyu M, Butburee T, Wang L. Stable hematite nanosheet photoanodes for enhanced photoelectrochemical watersplitting. Adv. Mater. 2016; 28:6405–5.
[27] Kay A, Cesar I, Grätzel M. New Benchmark for Water Photooxidation by Nanostructured α-Fe_2O_3 Films. J. Am. Chem. Soc. 2006; 128:15714-7.
[28] Gurudayal G, John RA, Boix PP, Yi C, Shi C, Scott MC, et. al. Atomically Altered Hematite for Highly Efficient Perovskite Tandem Water-Splitting Devices. CHEMSUSCHEM 2017; 10:2449-7.
[29] Maabong K, Machatine AGJ, Mwankemwa BS, Braun A, Bora DK, Toth R, et. al. Nanostructured hematite thin films for photoelectrochemical water splitting. Physica B 2018; 535:67-4.

[30] Annamalai A, Sandström R, Gracia-Espino E, Boulanger N, Boily J-F, Muehlbacher I, et al. Influence of Sb^{5+} as a Double Donor on Hematite (Fe^{3+}) Photoanodes for Surface-Enhanced Photoelectrochemical Water Oxidation. ACS Appl. Mater. Interfaces 2018; 10:16467-6.
[31] Tang PY, Xie HB, Ros C, Han LJ, Biset-Peiro M, He YM, et al. Enhanced photoelectrochemical water splitting of hematite multilayer nanowire photoanodes by tuning the surface state via bottom-up interfacial engineering. Energy& Environ. Sci. 2017; 10:2124-12.
[32] Kondofersky I, Dunn H, Müller A, Mandlmeier B, Feckl JM, Fattakhova-Rohlfing D, et al. Electron collection in host-guest nanostructured hematite photoanodes for water splitting: the influence of scaffold doping density. ACS Appl. Mater. Interfaces 2015; 7:4623-30.
[33] Stefik M, Cornuz M, Mathews N, Hisatomi T, Mhaisalkar S, Grätzel M. Transparent, Conducting Nb:SnO_2 for Host–Guest Photoelectrochemistry. Nano Lett. 2012; 12:5431-4.
[34] Sivula K, Le Formal F, Grätzel M. WO_3−Fe_2O_3 Photoanodes for Water Splitting: A Host Scaffold, Guest Absorber Approach. M. Chem. Mater. 2009; 21:2862-5.
[35] Itoh K, Bockris JO. Stacked thin-film photoelectrode using iron oxide. J. Appl. Phys. 1984; 56:874-7.
[36] Malviya KD, Dotan H, Shlenkevich D, Tsyganok A, Mora H, Rothschild A. Systematic comparison of different dopants in thin film hematite (α-Fe_2O_3) photoanodes for solar water splitting. J. Mater. Chem. A 2016; 4:3091-8.
[37] Annamalai A, Subramanian A, Kang U, Park H, Choi SH, Jang JS. Activation of Hematite Photoanodes for Solar Water Splitting: Effect of FTO Deformation. J. Phys. Chem. C 2015; 119:3810-7.
[38] Ling Y, Wang G, Wheeler DA, Zhang JZ, Li Y. Sn-Doped Hematite Nanostructures for Photoelectrochemical Water Splitting. Nano Lett. 2011; 5:2119-6.
[39] Ling Y, Li Y. Review of Sn-Doped Hematite Nanostructures for Photoelectrochemical Water Splitting. Particle&Particle Systems Characterization 2014; 31:1113-8.
[40] Sivula K, Le Formal F, Grätzel M. Solar Water Splitting: Progress Using Hematite (a-Fe_2O_3) Photoelectrodes. ChemSusChem 2011; 4:432-17.
[41] Patel P.P, Ghadge SD, Hanumantha PJ, Datta MK, Gattu B, Shanthi PM, Kumta PN. Active and robust novel bilayer photoanode architectures for hydrogen generation via direct non-electric bias induced photo-electrochemical water splitting. Int J. Hydrogen Energy 2018; 43:13158-8.
[42] Patel PP, Hanumantha PJ, Velikokhatnyi OI, Datta MK, Gattu B, Poston JA. Vertically aligned nitrogen doped (Sn,Nb)O_2 nanotubes – Robust photoanodes for hydrogen generation by photoelectrochemical water splitting. Mater. Sci. Eng. B 2016; 208:1-14.
[43] Patel PP, Hanumantha PJ, Velikokhatnyi OI, Datta MK, Hong D, Gattu B, et. al. Nitrogen and cobalt co-doped zinc oxide nanowires-Viable photoanodes for hydrogen generation via photoelectrochemical water splitting. J. Power Sources 2015; 299:11-14.
[44] Bondarchuk AN, Glot AB, Velasco-Rosales AR. Effects of Sb and Nb dopants on electrical and microstructural properties of low-voltage varistor ceramics based on SnO_2. Ceramics Internacional 2018; 44:7844-6.

[45] Tomás SA, Vigil O, Alvarado-Gil JJ, Lozada-Morales R, Zelaya-Angel O, Vargas H, et. al. Influence of thermal annealings in different atmospheres on the band-gap shift and resistivity of CdS thin films. J. Appl. Phys. 1995; 78:2204-13.
[46] Gilbert B, Frandsen C, Maxey ER, Sherman DM. Band-gap measurements of bulk and nanoscale hematite by soft x-ray spectroscopy. Phys. Rev. B 2009; 79:035108-7.
[47] Goyal RN, Pandey AK, Kaur D, Kumar A. Fabrication of alpha-Fe_2O_3 nanopowder modified glassy carbon electrode for applications in electrochemical sensing. J. Nanosci. Nanotechnol. 2009; 9:4692-7.
[48] Taffa DH, Hamm I, Dunkel C, Sinev I, Bahnemanncd D, Wark M. Electrochemical deposition of Fe_2O_3 in the presence of organic additives: a route to enhanced photoactivity. RSC Adv. 2015; 5:103512-10.

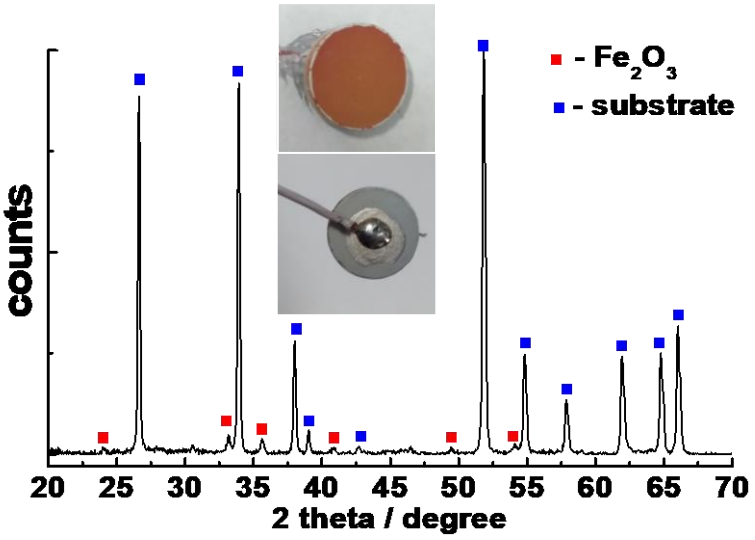

Fig.1. XRD pattern for the Fe_2O_3 photoelectrode grown on ceramic substrate. The image of its front and reverse sides is presented on the inset.

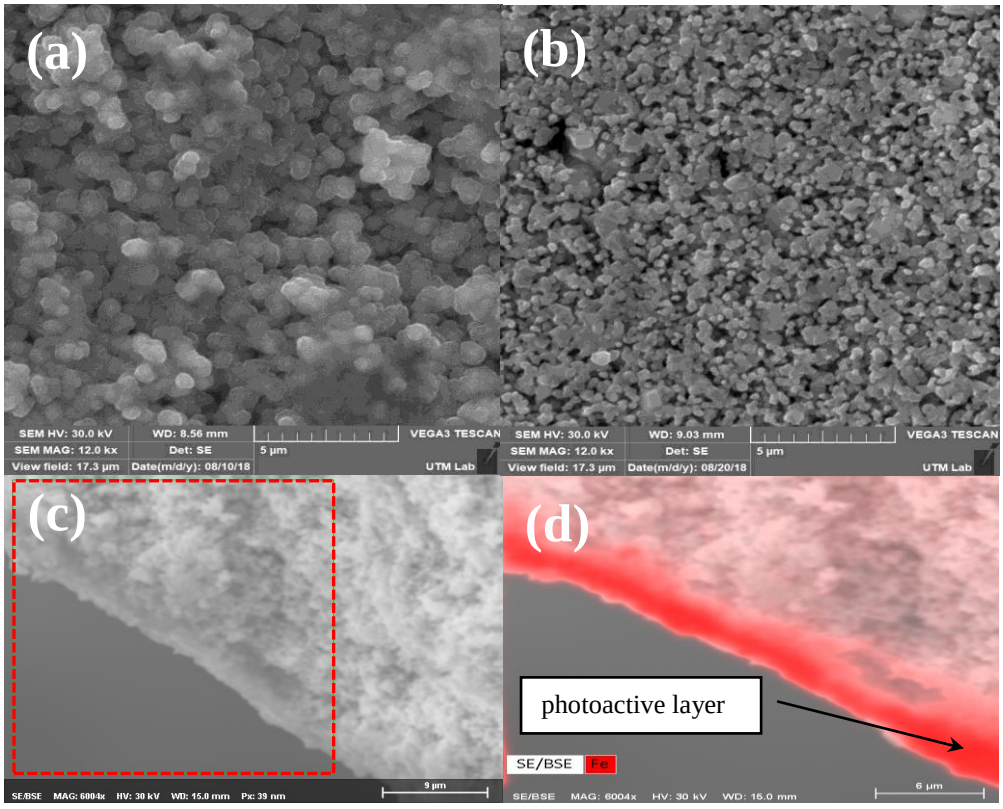

Fig.2. SEM micrographs of the photoelectrode: (a)hematite coating on SnO_2-Sb_2O_5 ceramics; (b)SnO_2-Sb_2O_5 ceramics on reverse side of photoelectrode; (c) cross-sectional of photoelectrode; (d) EDS elemental map of the Fe distribution in ceramic substrate for the selected area (red square) in (c).

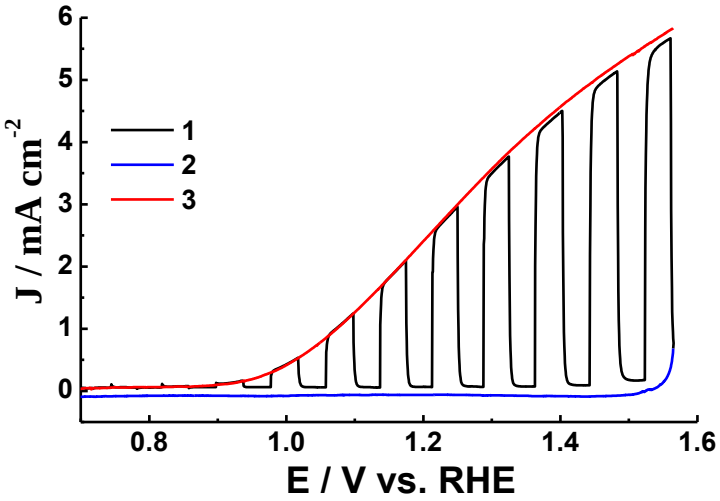

Fig.3. Cyclic voltammetry (scan rate 2.5 mV s^{-1}) for a hematite photoelectrode at the increase potential (curves 1 and 3) and its decrease (curve 2). Curve 1 was recorded under chopped blue light (0.03 Hz), curve 2 when the light was off (the dark current) and curve 3 when blue light was permanently on.

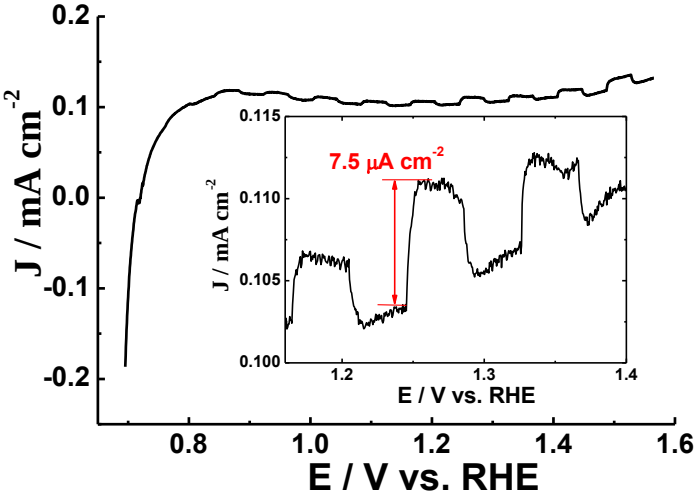

Fig.4. Cyclic voltammetry (scan rate 2.5 mV s^{-1}) for SnO_2-Sb_2O_5 ceramics under chopped blue light (0.03 Hz) at the increase potential. The inset presents a part of the same cyclic voltammetry in magnification.

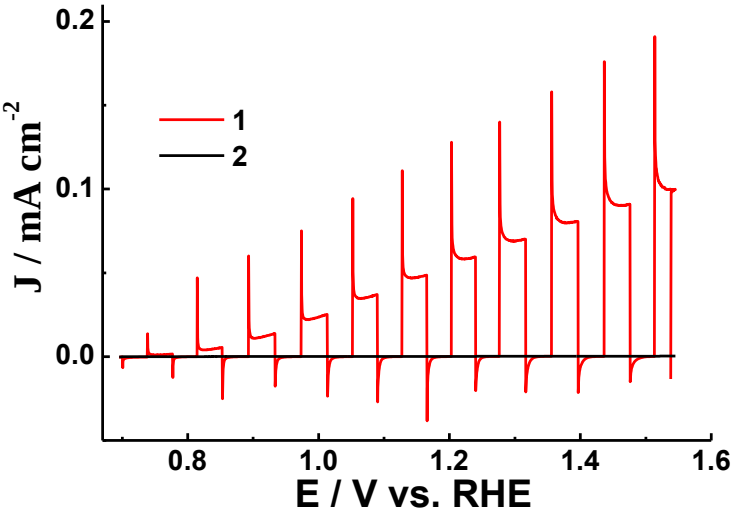

Fig.5. Cyclic voltammetry (scan rate 2.5 mV s^{-1}) for a hematite photoelectrode grown on ITO substrate at the increase potential (curve 1) and its decrease (curve 2). Curve 1 was recorded under chopped blue light (0.03 Hz), and curve 2 when light was off (the dark current).

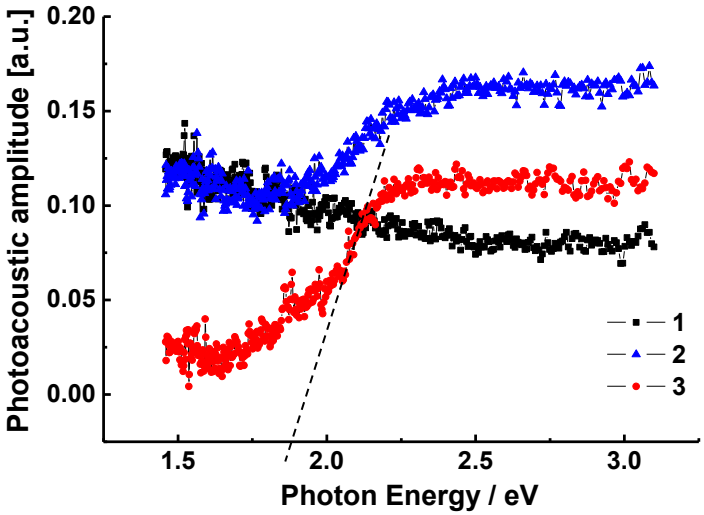

Fig.6. The photoacoustic spectra for the bare ceramic substrate (curve 1), for hematite electrode formed on the ceramic substrate (curve 2) and for hematite electrode grown on the ITO substrate (curve 3).